OBSERVATIONS OF THE YOUNG SUPERNOVA REMNANT RX J1713.7−3946 WITH THE *FERMI* LARGE AREA TELESCOPE

A. A. Abdo[1,61], M. Ackermann[2], M. Ajello[2], A. Allafort[2], L. Baldini[3], J. Ballet[4], G. Barbiellini[5,6], M. G. Baring[7], D. Bastieri[8,9], R. Bellazzini[3], B. Berenji[2], R. D. Blandford[2], E. D. Bloom[2], E. Bonamente[10,11], A. W. Borgland[2], A. Bouvier[12], T. J. Brandt[13,14,15], J. Bregeon[3], M. Brigida[16,17], P. Bruel[18], R. Buehler[2], S. Buson[8,9], G. A. Caliandro[19], R. A. Cameron[2], P. A. Caraveo[20], J. M. Casandjian[4], C. Cecchi[10,11], S. Chaty[4], A. Chekhtman[21,61], C. C. Cheung[22,61], J. Chiang[2], A. N. Cillis[23,24], S. Ciprini[11], R. Claus[2], J. Cohen-Tanugi[25], J. Conrad[26,27,62], S. Corbel[4,28], S. Cutini[29], A. de Angelis[30], F. de Palma[16,17], C. D. Dermer[31], S. W. Digel[2], E. do Couto e Silva[2], P. S. Drell[2], A. Drlica-Wagner[2], R. Dubois[2], D. Dumora[32], C. Favuzzi[16,17], E. C. Ferrara[24], P. Fortin[18], M. Frailis[30,33], Y. Fukazawa[34], Y. Fukui[35], S. Funk[2], P. Fusco[16,17], F. Gargano[17], D. Gasparrini[29], N. Gehrels[24], S. Germani[10,11], N. Giglietto[16,17], F. Giordano[16,17], M. Giroletti[36], T. Glanzman[2], G. Godfrey[2], I. A. Grenier[4], M.-H. Grondin[37], S. Guiriec[38], D. Hadasch[19], Y. Hanabata[34], A. K. Harding[24], M. Hayashida[2], K. Hayashi[34], E. Hays[24], D. Horan[18], M. S. Jackson[27,39], G. Jóhannesson[40], A. S. Johnson[2], T. Kamae[2], H. Katagiri[34], J. Kataoka[41], M. Kerr[2], J. Knödlseder[13,14], M. Kuss[3], J. Lande[2], L. Latronico[3], S.-H. Lee[2], M. Lemoine-Goumard[32,63], F. Longo[5,6], F. Loparco[16,17], M. N. Lovellette[31], P. Lubrano[10,11], G. M. Madejski[2], A. Makeev[1], M. N. Mazziotta[17], J. E. McEnery[24,42], P. F. Michelson[2], R. P. Mignani[43], W. Mitthumsiri[2], T. Mizuno[34], A. A. Moiseev[42,44], C. Monte[16,17], M. E. Monzani[2], A. Morselli[45], I. V. Moskalenko[2], S. Murgia[2], M. Naumann-Godo[4], P. L. Nolan[2], J. P. Norris[46], E. Nuss[25], T. Ohsugi[47], A. Okumura[48], E. Orlando[2,49], J. F. Ormes[46], D. Paneque[2,50], D. Parent[1], V. Pelassa[25], M. Pesce-Rollins[3], M. Pierbattista[4], F. Piron[25], T. A. Porter[2], S. Rainò[16,17], R. Rando[8,9], M. Razzano[3], O. Reimer[2,53], T. Reposeur[32], S. Ritz[12], R. W. Romani[2], M. Roth[54], H. F.-W. Sadrozinski[12], P. M. Saz Parkinson[12], C. Sgrò[3], D. A. Smith[32], P. D. Smith[15], G. Spandre[3], P. Spinelli[16,17], M. S. Strickman[31], H. Tajima[2], H. Takahashi[47], T. Takahashi[48], T. Tanaka[2], J. G. Thayer[2], J. B. Thayer[2], D. J. Thompson[24], L. Tibaldo[4,8,9,64], O. Tibolla[55], D. F. Torres[19,56], G. Tosti[10,11], A. Tramacere[2,57,58], E. Troja[24,65], Y. Uchiyama[2], J. Vandenbroucke[2], V. Vasileiou[25], G. Vianello[2,57], N. Vilchez[13,14], V. Vitale[45,59], A. P. Waite[2], P. Wang[2], B. L. Winer[15], K. S. Wood[31], H. Yamamoto[35], R. Yamazaki[60], Z. Yang[26,27], AND M. Ziegler[12]

[1] Center for Earth Observing and Space Research, College of Science, George Mason University, Fairfax, VA 22030, USA
[2] W. W. Hansen Experimental Physics Laboratory, Kavli Institute for Particle Astrophysics and Cosmology, Department of Physics and SLAC National Accelerator Laboratory, Stanford University, Stanford, CA 94305, USA; markusa@slac.stanford.edu, funk@slac.stanford.edu, uchiyama@slac.stanford.edu
[3] Istituto Nazionale di Fisica Nucleare, Sezione di Pisa, I-56127 Pisa, Italy
[4] Laboratoire AIM, CEA-IRFU/CNRS/Université Paris Diderot, Service d'Astrophysique, CEA Saclay, 91191 Gif sur Yvette, France
[5] Istituto Nazionale di Fisica Nucleare, Sezione di Trieste, I-34127 Trieste, Italy
[6] Dipartimento di Fisica, Università di Trieste, I-34127 Trieste, Italy
[7] Department of Physics and Astronomy, Rice University, Houston, TX 77251, USA
[8] Istituto Nazionale di Fisica Nucleare, Sezione di Padova, I-35131 Padova, Italy
[9] Dipartimento di Fisica "G. Galilei," Università di Padova, I-35131 Padova, Italy
[10] Istituto Nazionale di Fisica Nucleare, Sezione di Perugia, I-06123 Perugia, Italy
[11] Dipartimento di Fisica, Università degli Studi di Perugia, I-06123 Perugia, Italy
[12] Santa Cruz Institute for Particle Physics, Department of Physics and Department of Astronomy and Astrophysics, University of California at Santa Cruz, Santa Cruz, CA 95064, USA
[13] CNRS, IRAP, F-31028 Toulouse cedex 4, France
[14] Université de Toulouse, UPS-OMP, IRAP, Toulouse, France
[15] Department of Physics, Center for Cosmology and Astro-Particle Physics, The Ohio State University, Columbus, OH 43210, USA
[16] Dipartimento di Fisica "M. Merlin" dell'Università e del Politecnico di Bari, I-70126 Bari, Italy
[17] Istituto Nazionale di Fisica Nucleare, Sezione di Bari, 70126 Bari, Italy
[18] Laboratoire Leprince-Ringuet, École polytechnique, CNRS/IN2P3, Palaiseau, France
[19] Institut de Ciencies de l'Espai (IEEC-CSIC), Campus UAB, 08193 Barcelona, Spain
[20] INAF-Istituto di Astrofisica Spaziale e Fisica Cosmica, I-20133 Milano, Italy
[21] Artep Inc., Ellicott City, MD 21042, USA
[22] National Research Council Research Associate, National Academy of Sciences, Washington, DC 20001, USA
[23] Instituto de Astronomía y Fisica del Espacio, Parbellón IAFE, Cdad. Universitaria, Buenos Aires, Argentina
[24] NASA Goddard Space Flight Center, Greenbelt, MD 20771, USA
[25] Laboratoire de Physique Théorique et Astroparticules, Université Montpellier 2, CNRS/IN2P3, Montpellier, France
[26] Department of Physics, Stockholm University, AlbaNova, SE-106 91 Stockholm, Sweden
[27] The Oskar Klein Centre for Cosmoparticle Physics, AlbaNova, SE-106 91 Stockholm, Sweden
[28] Institut universitaire de France, 75005 Paris, France
[29] Agenzia Spaziale Italiana (ASI) Science Data Center, I-00044 Frascati (Roma), Italy
[30] Dipartimento di Fisica, Università di Udine and Istituto Nazionale di Fisica Nucleare, Sezione di Trieste, Gruppo Collegato di Udine, I-33100 Udine, Italy
[31] Space Science Division, Naval Research Laboratory, Washington, DC 20375, USA
[32] Université Bordeaux 1, CNRS/IN2p3, Centre d'Études Nucléaires de Bordeaux Gradignan, 33175 Gradignan, France
[33] Osservatorio Astronomico di Trieste, Istituto Nazionale di Astrofisica, I-34143 Trieste, Italy
[34] Department of Physical Sciences, Hiroshima University, Higashi-Hiroshima, Hiroshima 739-8526, Japan
[35] Department of Physics and Astrophysics, Nagoya University, Chikusa-ku Nagoya 464-8602, Japan
[36] INAF Istituto di Radioastronomia, 40129 Bologna, Italy
[37] Institut für Astronomie und Astrophysik, Universität Tübingen, D 72076 Tübingen, Germany
[38] Center for Space Plasma and Aeronomic Research (CSPAR), University of Alabama in Huntsville, Huntsville, AL 35899, USA
[39] Department of Physics, Royal Institute of Technology (KTH), AlbaNova, SE-106 91 Stockholm, Sweden

[40] Science Institute, University of Iceland, IS-107 Reykjavik, Iceland

[41] Research Institute for Science and Engineering, Waseda University, 3-4-1, Okubo, Shinjuku, Tokyo 169-8555, Japan

[42] Department of Physics and Department of Astronomy, University of Maryland, College Park, MD 20742, USA

[43] Mullard Space Science Laboratory, University College London, Holmbury St. Mary, Dorking, Surrey, RH5 6NT, UK

[44] Center for Research and Exploration in Space Science and Technology (CRESST) and NASA Goddard Space Flight Center, Greenbelt, MD 20771, USA

[45] Istituto Nazionale di Fisica Nucleare, Sezione di Roma "Tor Vergata," I-00133 Roma, Italy

[46] Department of Physics and Astronomy, University of Denver, Denver, CO 80208, USA

[47] Hiroshima Astrophysical Science Center, Hiroshima University, Higashi-Hiroshima, Hiroshima 739-8526, Japan

[48] Institute of Space and Astronautical Science, JAXA, 3-1-1 Yoshinodai, Chuo-ku, Sagamihara, Kanagawa 252-5210, Japan

[49] Max-Planck Institut für extraterrestrische Physik, 85748 Garching, Germany

[50] Max-Planck-Institut für Physik, D-80805 München, Germany

[51] Institut für Physik und Astronomie, Universität Potsdam, 14476 Potsdam, Germany

[52] Deutsches Elektronen Synchrotron DESY, D-15738 Zeuthen, Germany

[53] Institut für Astro- und Teilchenphysik and Institut für Theoretische Physik, Leopold-Franzens-Universität Innsbruck, A-6020 Innsbruck, Austria

[54] Department of Physics, University of Washington, Seattle, WA 98195-1560, USA

[55] Institut für Theoretische Physik and Astrophysik, Universität Würzburg, D-97074 Würzburg, Germany

[56] Institució Catalana de Recerca i Estudis Avançats (ICREA), Barcelona, Spain

[57] Consorzio Interuniversitario per la Fisica Spaziale (CIFS), I-10133 Torino, Italy

[58] INTEGRAL Science Data Centre, CH-1290 Versoix, Switzerland

[59] Dipartimento di Fisica, Università di Roma "Tor Vergata," I-00133 Roma, Italy

[60] Department of Physics and Mathematics, Aoyama Gakuin University, Sagamihara, Kanagawa, 252-5258, Japan

ABSTRACT

We present observations of the young supernova remnant (SNR) RX J1713.7−3946 with the *Fermi* Large Area Telescope (LAT). We clearly detect a source positionally coincident with the SNR. The source is extended with a best-fit extension of $0°55 \pm 0°04$ matching the size of the non-thermal X-ray and TeV gamma-ray emission from the remnant. The positional coincidence and the matching extended emission allow us to identify the LAT source with SNR RX J1713.7−3946. The spectrum of the source can be described by a very hard power law with a photon index of $\Gamma = 1.5 \pm 0.1$ that coincides in normalization with the steeper H.E.S.S.-detected gamma-ray spectrum at higher energies. The broadband gamma-ray emission is consistent with a leptonic origin as the dominant mechanism for the gamma-ray emission.

Key words: acceleration of particles – gamma rays: general – gamma rays: ISM – ISM: individual objects (RX J1713.7-3946) – ISM: supernova remnants – radiation mechanisms: non-thermal

Online-only material: color figures

1. INTRODUCTION

Gamma-ray observations of shell-type supernova remnants (SNRs) hold great promise of helping us to understand the acceleration of cosmic rays (CRs). These particles—arriving at Earth mostly in the form of protons—are thought to be accelerated by a mechanism called diffusive shock acceleration (DSA; Bell 1978; Blandford & Ostriker 1978; Jones & Ellison 1991; Malkov & Drury 2001) in the shocks of supernova (SN) explosions up to energies around the "knee" in the spectrum of CRs ($\sim 10^{15}$ eV). In particular, X-ray and TeV gamma-ray observations of young SNRs such as Cas A (Hwang et al. 2004; Gotthelf et al. 2001; Albert et al. 2007; Abdo et al. 2010b) or RX J1713.7−3946 (Koyama et al. 1997; Uchiyama et al. 2007; Aharonian et al. 2006, 2007) have confirmed the existence of relativistic particles in the shock waves. Young SNRs are preferred targets for seeing particle acceleration at work since in these objects the shocks are still strong and actively accelerating particles to the highest energies. Gamma-ray instruments have the angular resolution to spatially resolve some of the closer SNRs.

RX J1713.7−3946 (also known as G347.3−0.5) is a young "historical" remnant suggested to be associated with the appearance of a guest star in the constellation of Scorpius in AD393 by Wang et al. (1997). RX J1713.7−3946 is located in the Galactic plane (at $l = 347°3$, $b = −0°5$) and was discovered in soft X-rays in 1996 in the *ROSAT* all-sky survey (Pfeffermann & Aschenbach 1996). At a suggested distance of 1 kpc (Koyama et al. 1997; Fukui et al. 2003; Cassam-Chenaï et al. 2004) with angular diameter $\sim 65' \times 55'$, the size of the shell is ~ 20 pc. Its properties are strikingly dominated by non-thermal activity. Its X-ray emission shows a featureless spectrum interpreted to be completely dominated by X-ray synchrotron emission from ultra-relativistic electrons (Koyama et al. 1997; Slane et al. 1999; Tanaka et al. 2008). The thermal X-ray emission as well as the radio emission are extremely faint (Lazendic et al. 2004). Detailed X-ray observations with *Chandra* and *XMM-Newton* unveiled a complex structure of filaments and knots in the shell of the SNR—in particular in the western part (Uchiyama et al. 2003; Lazendic et al. 2004; Cassam-Chenaï et al. 2004; Acero et al. 2009). A recent study with the *Suzaku* satellite extended the X-ray spectrum to ~ 40 keV, a measurement that enabled the determination of the parent electron spectrum in the energy range where the spectrum cuts off (Tanaka et al. 2008).

RX J1713.7−3946 is the first SNR for which TeV gamma-ray emission was clearly detected emerging from the shell. H.E.S.S. measurements provided the first-ever resolved gamma-ray emission at TeV energies. The TeV emission closely matches the non-thermal X-ray emission as demonstrated by Aharonian et al. (2006). The energy spectrum of RX J1713.7−3946 has been measured up to ~ 100 TeV, clearly demonstrating particle acceleration to beyond these energies in the shell of the SNR.

While the non-thermal X-rays detected in the shells of young SNRs are clearly generated through synchrotron emission by ultra-relativistic electrons (Koyama et al. 1997), the picture of the particle population radiating the gamma rays is not so clear. The main argument revolves around two main emission mechanisms (Aharonian et al. 2006; Katz & Waxman 2008; Berezhko & Völk 2008; Porter et al. 2006; Ellison & Vladimirov 2008; Morlino et al. 2009), but so far, conclusive evidence for either possibility is still missing. One scenario suggests a connection of the TeV gamma-ray emission with accelerated protons (CRs) by invoking the interaction of these protons with interstellar material generating neutral pions (π^0s) which in turn decay into gamma rays. A second competing channel exists in the inverse Compton (IC) scattering of the photon fields in the surroundings of the SNR by the same relativistic electrons that generate the synchrotron X-ray emission. This channel naturally accounts for the close resemblance between the X-ray and the TeV gamma-ray images. Several ways have been suggested to distinguish between these two scenarios (see, e.g., Morlino et al. 2009) but one of the most promising seems to be the broadband modeling of the spectral energy distribution (SED). In this regard, observations of young SNRs with the Large Area Telescope (LAT) on board the *Fermi Gamma-Ray Space Telescope* are of particular importance since the LAT detects gamma rays in the energy range that bridges sensitive measurements with X-ray satellites such as *Chandra* and *XMM-Newton* and TeV gamma-ray telescopes such as H.E.S.S., VERITAS, or MAGIC.

2. OBSERVATION AND ANALYSIS

The *Fermi*-LAT is a pair-conversion gamma-ray telescope with a precision tracker and calorimeter, each consisting of a 4×4 array of 16 modules, a segmented anti-coincidence detector (ACD) that covers the tracker array, and a programmable trigger and data acquisition system. The incoming gamma rays produce electron–positron pairs in the tracker subsystem, which allow a reconstruction of the directions of the primary gamma rays using the information provided by the 36 layers of silicon strip detectors in the tracker. The energy of the incoming gamma ray is determined from the energy deposited by the electromagnetic showers in the segmented CsI calorimeter. The ACD subsystem is used as a veto against the great majority of CRs that trigger the LAT. The energy range of the LAT is 20 MeV to >300 GeV with an angular resolution for events converting in the front part of the detector of approximately 3°.5 at 100 MeV, improving to about 0°.1 at 10 GeV (defined as the 68% containment radius of the LAT point-spread function (PSF)). Full details on the instrument and the on-board and ground data processing are given in Atwood et al. (2009).

The LAT normally operates in a scanning mode (the "sky survey" mode) that covers the whole sky every two orbits (~3 hr). We use data taken in this mode from the commencement of scientific operations on 2008 August 4 to 2010 August 4. The data were prepared and analyzed using the LAT Science Tools package (v9r16p1), which is available from the *Fermi* Science Support Center.[66] Only events satisfying the standard low-background event selection (the so-called Diffuse class events) and coming from zenith angles <105° (to greatly reduce the contribution by Earth albedo gamma rays; see Abdo et al. 2009a) were used in the present analysis. We used all gamma rays with energy >500 MeV within a $20° \times 20°$ region of interest

(ROI) centered at the nominal position of RX J1713.7−3946 ($\alpha = 258°.39$, $\delta = 39°.76$). We chose a lower bound of 500 MeV for this analysis for two reasons: due to the relative hardness of the spectrum of RX J1713.7−3946 compared to the Galactic diffuse background, photons with energies below 500 MeV are not effective in constraining the morphology or spectral shape of the source. Additionally, the broadening of the PSF at low energies might lead to systematic problems of confusion with neighboring sources in this densely populated region of the sky. To further reduce the effect of Earth albedo backgrounds, any time intervals when the Earth was appreciably in the field of view (specifically, when the center of the field of view was more than 52° from the zenith) as well as any time intervals when parts of the ROI were observed at zenith angles >105° were also excluded from the analysis. The spectral analysis was performed based on the P6v3 version of post-launch instrument response functions which take into account pile-up and accidental coincidence effects in the detector subsystems (Rando et al. 2010). The binned maximum likelihood mode of *gtlike*, which is part of the ScienceTools, was used to determine the intensities and spectral parameters presented in this paper.
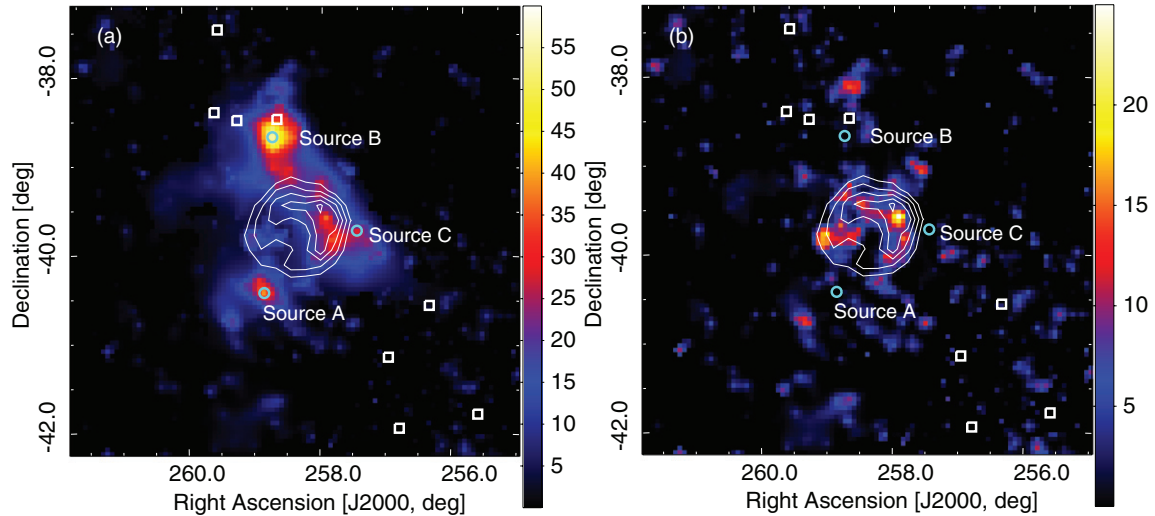
2.1. Background Sources

We adopt a background model for the region which includes components describing the diffuse Galactic and isotropic gamma-ray emission.[67] It also includes all point sources within our ROI that are identified in the 1FGL catalog (Abdo et al. 2010a) except for 1FGL 1711.7−3944c which is spatially coincident with RX J1713.7−3946. All 1FGL sources are modeled with a power-law spectrum using the flux and spectral index values obtained from the catalog. Exceptions are the known pulsars in the ROI which we model with a power law with an exponential cutoff spectral model. As the parameters for this spectral model cannot be obtained from the 1FGL catalog, we keep the flux, spectral index, and cutoff energy of the known pulsars as free parameters in the maximum likelihood fits of the ROI. Figure 1 shows two maps of the point-source detection significance, evaluated at each point in the map (TS map) for the region around RX J1713.7−3946 using photons with energies >500 MeV. The flux of the source is not permitted to be negative; this is why negative fluctuations are not visible. The detection significance is shown in terms of the test statistic (TS) of the likelihood fit. The TS value is defined as TS = $2(\ln L_1/L_0)$, proportional to the logarithm of the likelihood ratio between a point-source hypothesis (L_1) and the null hypothesis of pure background (L_0) (Mattox et al. 1996). The significance contours of the TeV emission observed from the SNR by the H.E.S.S. telescope array (Aharonian et al. 2006) are overlaid on the maps. Panel (a) shows the TS map characterizing the excess emission found in the region around RX J1713.7−3946 over our background model described above. A significant TS value is found within the spatial extent of the SNR but also in several regions outside of its shell.

We identify three regions of excess gamma-ray emission which are likely not associated with the SNR but belong to background sources not recognized in the first *Fermi* catalog (1FGL). Due to the longer integration time of our analysis (24 months versus 11 months in the catalog) and the corresponding improved sensitivity, the appearance of additional sources

---

Figure 1. (a) Map of the test statistic (TS) for a point source in the region around RX J1713.7−3946 obtained in a maximum likelihood fit accounting for the background diffuse emission and 1FGL catalog sources. Only events above 500 MeV have been used in this analysis. H.E.S.S. TeV emission contours are shown in white (Aharonian et al. 2007). Rectangles indicate the positions of 1FGL sources in our background model. Several TS peaks outside the SNR shell are visible. The three peaks marked by circles are added as additional sources to our background model (see the text). (b) Same map as panel (a), but with the three additional sources now considered in the background model.

(A color version of this figure is available in the online journal.)

in our ROI is expected. We simply denote these sources with the identifiers *A, B, C*. The source positions are shown in Figure 1 and given in Table 2. The location of source *A* is consistent with a weak radio source (Lazendic et al. 2004). It is further identified in an internal update of the *Fermi*-LAT catalog using 24 months of data. Source *B* is only 11′ from the catalog source 1FGL J1714.5−3830c and could be an artifact caused by unmodeled emission from 1FGL J1714.5−3830c if this source is spatially extended as has been tentatively suggested by Castro & Slane (2010). 1FGL J1714.5−3830c is modeled as a point source in the 1FGL catalog. However, the catalog source is spatially coincident with SNR CTB 37A which has an extent in radio of ~15′ (Green 2004). A detailed study of the morphology of this source is in progress but beyond the scope of this publication as the exact morphology of CTB 37A does not significantly affect the spectral analysis of RX J1713.7−3946. For simplicity we just assume the emission from this region can be described by two independent point sources, 1FGL J1714.5−3830c and source *B*. The third additional background source *C* shown in Figure 1 may be associated with RX J1713.7−3946. It is very close to RX J1713.7−3946, located about 35′ from the center of the SNR. However, it is spatially consistent with a local enhancement of molecular gas, observed via the radio emission from the CO ($J = 1 \rightarrow 0$) transition (Dame et al. 2001). Furthermore, we will show below (see Table 2) that in a combined likelihood analysis of the spectra of RX J1713.7−3946 and the surrounding background sources the emission from source *C* is considerably softer than the gamma-ray emission from the SNR. In fact, both the spectral index and the intensity of the source are consistent with expectations of gamma-ray emission from a small cloud of molecular gas. Nevertheless, we cannot reject the possibility that at least part of the emission attributed to the additional background source *C* is originating from the SNR shell. While we consider source *C* an independent point source in our standard background model of the ROI, we repeat the spectral analysis with a model without this source and account for the difference in our estimation of systematic uncertainties. Figure 1(b) shows the detection significance map for the region around RX J1713.7−3946 ($E >$

500 MeV) with our standard background model accounted for. A comparison with the significance contours from H.E.S.S. suggests a spatially extended emission from the shell of the SNR rather than a single point source.

2.2. Centroid and Angular Extent

We study the morphology of the emission associated with RX J1713.7−3946 with a series of maximum likelihood fits, comparing the TS value for different hypotheses about the shape and extent of the source. We fitted the extension (and position) of the gamma-ray emission with a disk of varying radius. The emission is found to be significantly extended; the best-fit position (R.A., decl. $= 258°50 \pm 0°04_{stat}, -39°91 \pm 0°05_{stat}$) is consistent with the center of the SNR within $0°2$ and the best-fit radius is $0°55 \pm 0°04$. This size is consistent with that of the X-ray SNR given in Green (2004) as $1°1 \times 0°9$ in diameter. To confirm these fits, we test a single point source at the location of the highest excess in the TS map within the shell of the SNR. We further test a spatially extended source defined by the shape of the H.E.S.S. significance contours of RX J1713.7−3946 and an extended source as a uniform disk of $0°55$ radius. Finally, we consider two and three independent point sources within the shell of the SNR located at the most prominent peaks in the TS map. A power-law spectrum with integrated flux (between 1 and 300 GeV) and spectral index as free parameters is assumed for each of the hypotheses. The detailed setup of the likelihood fit is identical to the one used for the spectral analysis and described with that analysis (Section 2.3). Table 1 shows the flux, and spectral index of the tested shape and its TS value in comparison to the background model. The TS values are suggestive of extended gamma-ray emission from RX J1713.7−3946. The H.E.S.S. significance map as well as the uniform disk have a difference in TS of ΔTS $= 61$ or 58 (H.E.S.S./Disk) relative to a single point source and a ΔTS $= 43$ or 40 (H.E.S.S./ Disk) relative to a set of three point sources within the shell of RX J1713.7−3946. However, the TS value in a comparison to the background model for both the H.E.S.S. significance map (TS $= 77$) and the uniform disk (TS $= 79$) is almost identical, demonstrating that we are not sensitive to the detailed shape

Table 1
Results of the Morphological Analysis of the Gamma-ray Emission from RX J1713.7−3946

Source Morphology	Flux[a]	Photon Index	TS[b]	R.A. 2000	Decl.
Point source	1.2 ± 0.7	1.85 ± 0.31	18	257°.94	−39°.75
Two point sources	0.5 ± 0.5	1.68 ± 0.41		257°.93	−39°.61
	1.2 ± 0.9	2.13 ± 0.41	20	257°.85	−39°.86
Three point sources	0.5 ± 0.5	1.69 ± 0.41		257°.93	−39°.61
	1.2 ± 0.2	2.10 ± 0.28		257°.85	−39°.86
	0.4 ± 0.3	1.61 ± 0.31	32	259°.00	−39°.81
Extended source (H.E.S.S.)[c]	2.8 ± 0.7	1.50 ± 0.11	77		
Extended source (uniform disk)[d]	3.2 ± 0.7	1.49 ± 0.10	79	258°.50	−39°.91

Notes. The integral flux between 1 and 300 GeV and the spectral index are the free parameters of the fit and are fitted in the energy range 500 MeV to 400 GeV.
[a] $E > 1$ GeV, in 10^{-9} cm^{-2} s^{-1}.
[b] TS value in comparison to a model with no source at the position of RX J1713.7−3946.
[c] H.E.S.S. significance map is used as a template for the intensity of the gamma-ray emission.
[d] A uniform disk with 0°.55 radius is used as a template for the intensity of the gamma-ray emission. The specified coordinates correspond to the center of the disk. These parameters are the best-fit parameters when simultaneously fitting the position and the extension.

of the emission region. For the models of RX J1713.7−3946 considered, the TS value is expected to follow a χ^2 distribution with two degrees of freedom in the case where no source is present (Mattox et al. 1996) and therefore can be converted to a detection significance of ∼8.5σ for both the H.E.S.S. template and the uniform disk model. The positional and the angular-size coincidence with the X-ray and TeV gamma-ray emission strongly favors an identification of the LAT source with SNR RX J1713.7−3946.

Figure 2 shows a series of LAT gamma-ray count maps of the sky surrounding RX J1713.7−3946. We choose an energy threshold of 3 GeV for these maps, higher than the analysis threshold of 500 MeV, to enhance their resolution. The count maps are smoothed with a 0°.3 wide Gaussian kernel. This width corresponds to the size of the LAT PSF at 3 GeV (the 39% containment radius of a two-dimensional Gaussian), averaged over front and back conversions and over all incident angles. Locations of 1FGL catalog sources in the region are marked by squares. Our additional background sources are denoted by circles and labeled. The black lines again display the contours of the H.E.S.S. significance map of RX J1713.7−3946. Panel (a) shows all counts in the region. The emission coinciding with RX J1713.7−3946 is faint; the counts map is dominated by the Galactic diffuse emission as well as emission from 1FGL J1714.5−3830c and 1FGL J1705.5−4034c. Panel (b) shows a residual counts map after subtraction of our background model. On this panel, a clear excess within the shell of RX J1713.7−3946 is visible. Panel (c) finally shows the residual counts after subtraction of our background model as well as the emission from RX J1713.7−3946 (using the H.E.S.S. significance map as the template for the spatial extension). The residual counts are consistent with the expected statistical fluctuations, i.e., the region around the SNR is well described by our model.

2.3. Spectral Analysis

We adopt the spatial extension model based on the H.E.S.S. significance map as the default model for the analysis of the spectrum of RX J1713.7−3946. As discussed in the previous section, LAT is not able to distinguish between the two extended source models that we tested. Therefore, we compare the obtained spectrum from the default model to the results derived from a uniform disk source model and include the dif-

ference in the systematic uncertainty of the spectrum. In the first step of the spectral analysis, we perform a maximum likelihood fit of the spectrum of RX J1713.7−3946 in the energy range between 500 MeV and 400 GeV using a power-law spectral model with integral flux and spectral index as free parameters. To accurately account for correlations between close-by sources, we also allow the integral fluxes and spectral indices of the nearby 1FGL and sources *A, B, C* (<3° from the center of the ROI) to be free for the likelihood maximization, as well as the spectral parameters of identified LAT pulsars, instead of fixing them to the 1FGL catalog values. We redetermine in our fit the normalization of the Galactic diffuse emission model, the index of an energy-dependent (power-law) multiplicative correction factor to it, and the normalization of the isotropic component. This accounts for localized variations in the spectrum of the diffuse emission in the fit which are not considered in the global model.

For the Galactic diffuse emission, we find a normalization factor of 0.93 ± 0.01 in our ROI and a spectral correction factor index of 0.019 ± 0.002 (the positive sign corresponds to a spectrum that is harder than in the model). The normalization factor for the isotropic component is 1.17 ± 0.05. These factors demonstrate the good agreement of the local brightness and spectrum of the diffuse gamma-ray emission with the global diffuse emission model. Table 2 summarizes the source parameters obtained as results from this fit. The table includes the spectral parameters and the TS values of all fitted sources. The flux above 1 GeV obtained for RX J1713.7−3946 with our default background model is $F_{1000} = (2.8 \pm 0.7) \times 10^{-9}$ cm^{-2} s^{-1} and the spectral index is $\Gamma = 1.50 \pm 0.11$. Figure 3 shows the uncertainty band obtained from this fit.

In a second step, we perform a maximum likelihood fit of the flux of RX J1713.7−3946 in seven independent logarithmically spaced energy bands from 500 MeV to 400 GeV (using the spectral model and parameters obtained in the previous fit) to obtain an SED for the SNR. The resulting SED is displayed in Figure 3 as black error bars. We require a TS value of TS ⩾ 4 in each band to draw a data point corresponding to a 2σ detection significance. This criterion is not fulfilled for the lowest two energy bands 500 MeV–1.3 GeV and 1.3 GeV–3.4 GeV and accordingly we show 95% flux upper limits for these bands.

In a final step we estimate the systematic uncertainty on the obtained spectral parameters by repeating the maximum
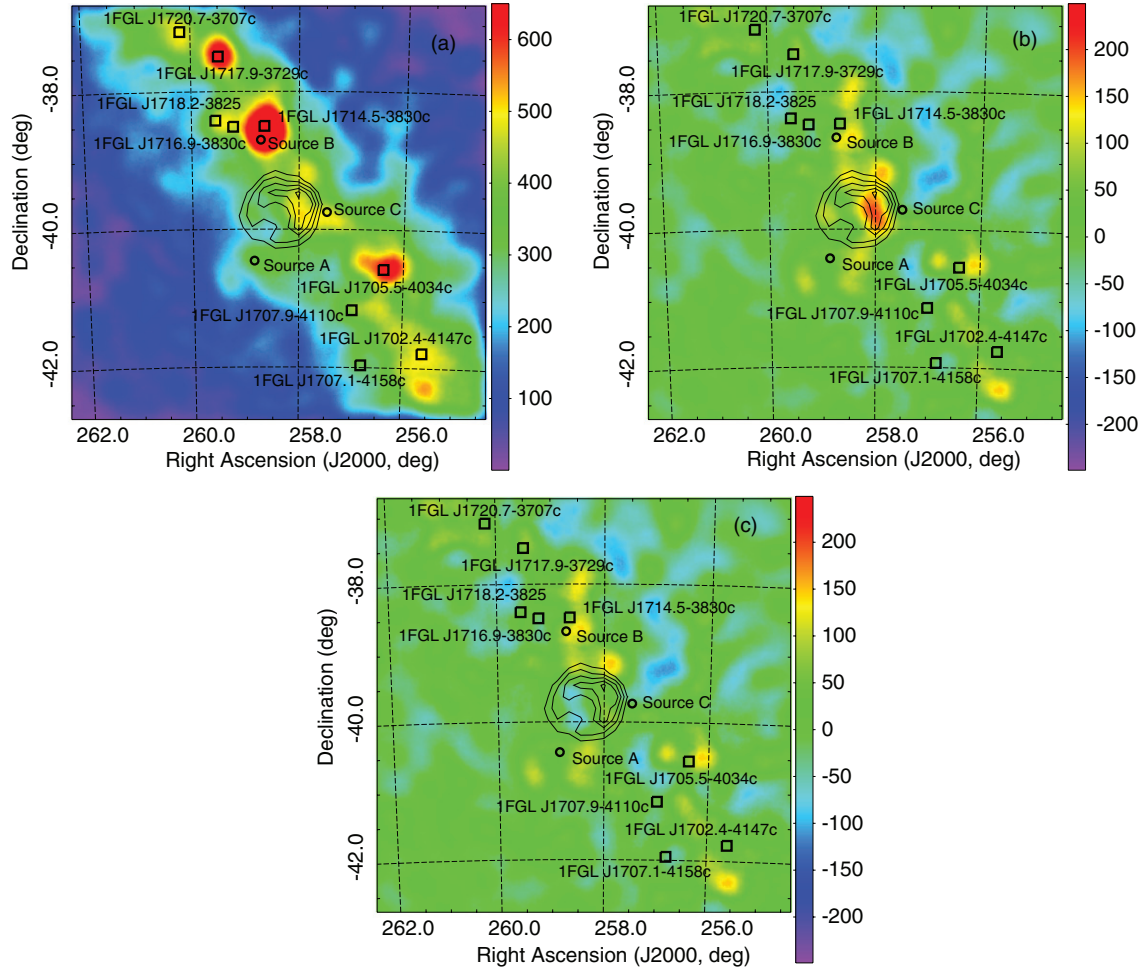
Figure 2. (a) Counts deg^{-2} observed by the *Fermi*-LAT above 3 GeV in the region around RX J1713.7−3946. The map is smoothed with a 0°3 wide Gaussian kernel corresponding to the width of the LAT PSF at 3 GeV. H.E.S.S. TeV emission contours are shown in black (Aharonian et al. 2007). Rectangles indicate the positions of 1FGL sources. Circles indicate the additional sources considered in our background model. (b) Residual counts after the subtraction of the counts attributed to the background model. (c) Residual counts after the subtraction of the counts attributed to the background model and to RX J1713.7−3946.

(A color version of this figure is available in the online journal.)

Table 2
Results of the Spectral Analysis of the Gamma-ray Emission in the ROI Centered at RX J1713.7−3946

Source Name	Flux[a]	Photon Index	Exp. Cutoff[b]	TS[c]	R.A. 2000	Decl.
1FGL J1705.5−4034c	2.1 ± 0.7	2.16 ± 0.19		20		
1FGL J1709.7−4429	175 ± 6.4	1.74 ± 0.03	4.46 ± 0.23	50064		
1FGL J1714.5−3830c	9.8 ± 1.3	2.47 ± 0.09		228		
1FGL J1716.9−3830c	1.9 ± 1.1	2.47 ± 0.34		14		
1FGL J1717.9−3729c	4.9 ± 0.7	2.34 ± 0.11		81		
1FGL J1718.2−3825	8.4 ± 4.3	1.64 ± 0.41	1.72 ± 0.65	165		
Source A	1.6 ± 0.5	2.03 ± 0.17		28	258°84	−40°46
Source B	4.2 ± 1.2	2.48 ± 0.16		43	258°71	−38°70
Source C	2.5 ± 0.7	2.45 ± 0.22		21	257°47	−39°75
RX J1713.7−3946	2.8 ± 0.7	1.50 ± 0.11		77		

Notes. The integral flux between 1 and 300 GeV and the spectral index are the free parameters of the fit and are fitted in the energy range 500 MeV to 400 GeV.
[a] $E > 1$ GeV, in 10^{-9} cm^{-2} s^{-1}.
[b] In GeV.
[c] Difference in TS value in comparison to a model with no source at the position of the respective source.

likelihood analysis for several variations of our default model. Specifically, we varied the source shape template, the background sources, and the model of the Galactic diffuse emission. The spectral analysis was performed: (1) with the uniform disk shape replacing the H.E.S.S. significance map template,

(2) with the closest background source *C* removed from the model (see also the discussion above), (3) using a preliminary list of sources from the 2FGL catalog in development within the LAT collaboration, (4) replacing the standard diffuse emission model by a refined model that is currently being evaluated
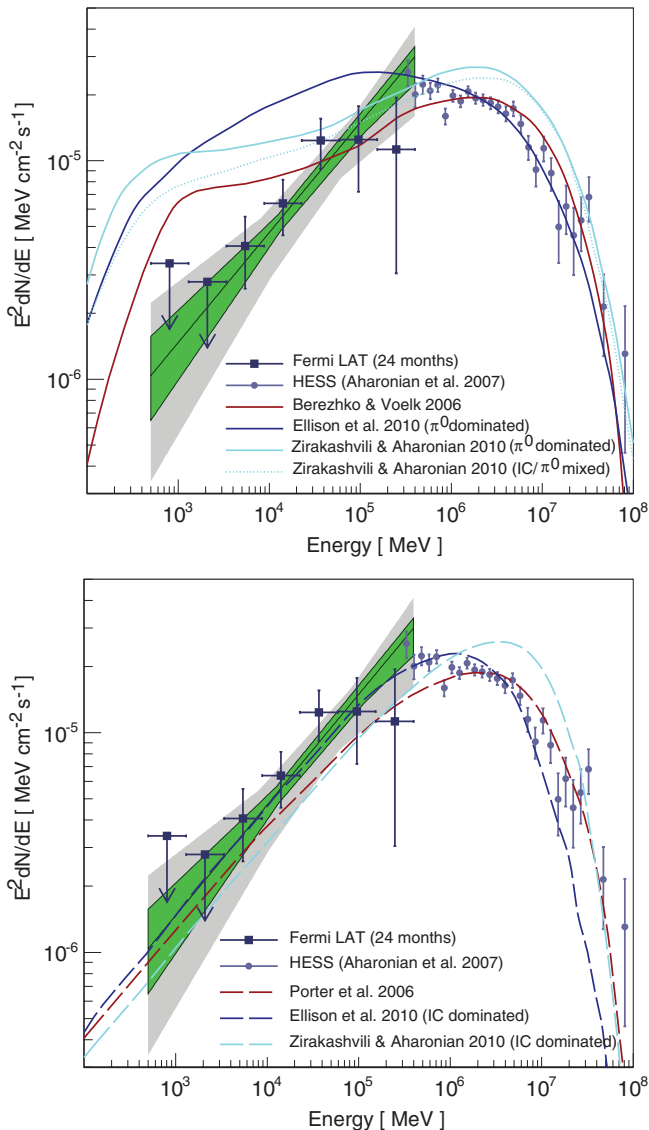
Figure 3. Energy spectrum of RX J1713.7−3946 in gamma rays. Shown is the *Fermi*-LAT-detected emission in combination with the energy spectrum detected by H.E.S.S. (Aharonian et al. 2007). The green region shows the uncertainty band obtained from our maximum likelihood fit of the spectrum of RX J1713.7−3946 assuming a power law between 500 MeV and 400 GeV for the default model of the region. The gray region depicts the systematic uncertainty of this fit obtained by variation of the background and source models. The black error bars correspond to independent fits of the flux of RX J1713.7−3946 in the respective energy bands. Upper limits are set at a 95% confidence level. Also shown are curves that cover the range of models proposed for this object. These models have been generated to match the TeV emission and pre-date the LAT detection. The top panel features predictions assuming that the gamma-ray emission predominately originates from the interaction of protons with interstellar gas (brown: Berezhko & Völk 2006; blue: Ellison & Vladimirov 2008; cyan (solid/dashed): Zirakashvili & Aharonian 2010). The bottom panel features models where the bulk of the gamma-ray emission arises from interactions of electrons with the interstellar radiation field (leptonic models). (Brown: Porter et al. 2006; blue: Ellison & Vladimirov 2008; cyan: Zirakashvili & Aharonian 2010.) See the text for a qualitative discussion of these models. It should be noted that the publication of the latest H.E.S.S. spectrum (Aharonian et al. 2007) contains a mismatch between Table 5 and Figure 4 by a factor of 0.85 (Figure 4 is correct, the table values have to be multiplied by 0.85 to get the correct values). Some of the mismatch between model curves (e.g., Zirakashvili & Aharonian 2010) and the H.E.S.S. data might be due to this discrepancy.

(A color version of this figure is available in the online journal.)

in the collaboration for source analysis for the 2FGL catalog (refined with 24 months of data and with finer gas maps), and

(5) replacing the standard diffuse model by a model based on the GALPROP code[68] used in the *Fermi*-LAT analysis of the isotropic diffuse emission. The GALPROP model is described in Abdo et al. (2010c). For (5), i.e., the GALPROP-based model, we considered the various components of the diffuse emission model separately for which we then individually fit the normalizations in our likelihood analysis. The components are gamma rays produced by IC emission, gamma rays produced by interactions of CRs with atomic and ionized interstellar gas, and gamma rays produced in the interactions of CRs with molecular gas. The model component describing the gamma-ray intensity from interactions with molecular gas is further subdivided into seven ranges of Galactocentric distance to accommodate localized variations of the CR and molecular gas density along the line of sight which are not accounted for in the model.

The same model of the isotropic component was used for all model variations (1)–(5). From model variations (1)–(5), we obtain a systematic uncertainty of +0.08/−0.10 for the spectral index of RX J1713.7−3946 and a systematic uncertainty of $(+0.6/-0.7) \times 10^{-9}$ cm^{-2} s^{-1} for the flux above 1 GeV on top of the statistical uncertainty. The systematic uncertainty of the derived flux and spectral index related to the uncertainty in the LAT effective area was evaluated separately. The uncertainty of the LAT effective area—estimated from observations of Vela (Abdo et al. 2009b) and the Earth albedo (Abdo et al. 2009a)—ranges from 10% at 500 MeV to 20% at ⩾10 GeV. The impact on the spectral parameters of RX J1713.7−3946 is a systematic uncertainty of ±0.05 for the spectral index and a systematic uncertainty of ±0.4 for the flux above 1 GeV. The gray band in Figure 3 displays the superposition of all uncertainty bands obtained in our variations of the default model. Figure 4 depicts the model variation (2) resulting in the softest spectrum together with the fluxes in individual energy bands (black error bars) derived for model (2) using the same procedure as for the default model described above. The range of systematic uncertainty is particularly important to consider for comparisons of the spectrum to pion-decay-dominated gamma-ray emission models which are generally expected to be softer than IC-dominated gamma-ray emission models.

3. DISCUSSION

The positional coincidence between the extended gamma-ray emission detected by the *Fermi*-LAT at the position of RX J1713.7−3946 strongly suggests a physical association between the GeV gamma-ray emission and this young SNR. In addition, the region of brightest LAT gamma-ray emission coincides with the northwestern part of the SNR. From CO ($J = 1$–0) observations, Fukui et al. (2003) and Moriguchi et al. (2005) suggested that this part of the SNR is undergoing complex interactions between the SN shock wave and a molecular cloud. This part is also the brightest region in non-thermal X-rays and in TeV gamma rays. The match between the locations of brightest emission suggests that the GeV emission is also generated by the population of relativistic particles responsible for the TeV gamma-ray and non-thermal X-ray emission.

The origin of the TeV gamma-ray emission from RX J1713.7−3946 has been a matter of active debate (see Zirakashvili & Aharonian 2010, and references therein). There are two competing processes potentially responsible for the

---

[68] GALPROP is a software package for calculating the diffuse Galactic gamma-ray emission based on a model of cosmic-ray propagation in the Galaxy. See http://galprop.stanford.edu/ for details and references.
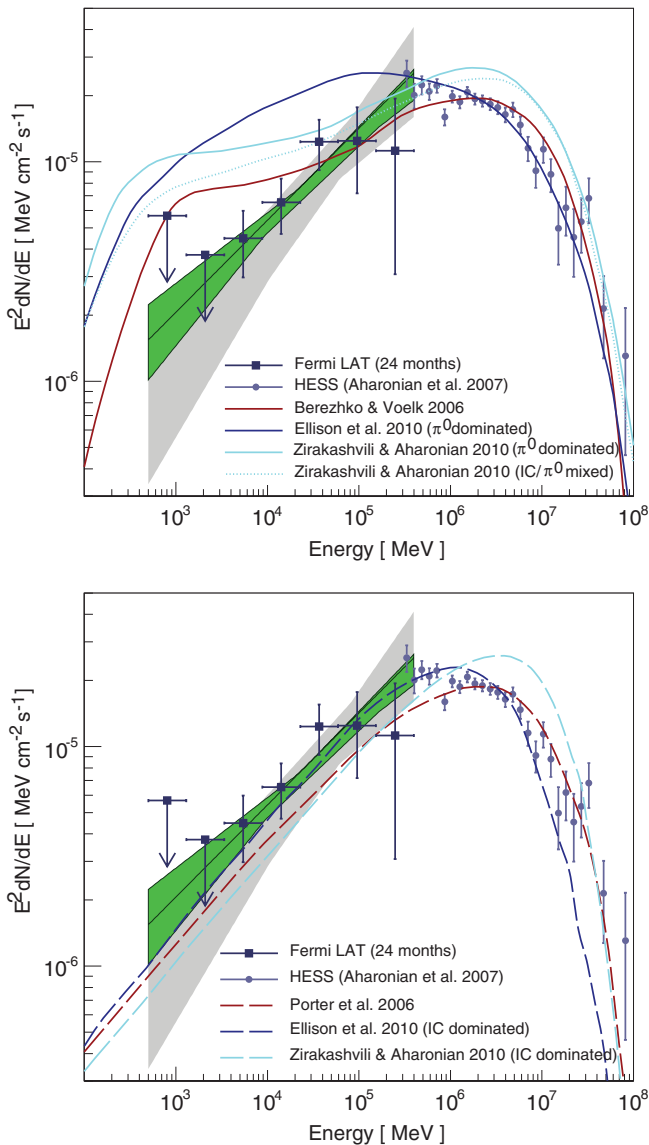
Figure 4. Same as Figure 3 but featuring the source and background model which resulted in the softest spectrum for RX J1713.7−3946 instead of our default model.

(A color version of this figure is available in the online journal.)

shell-like TeV gamma-ray emission from RX J1713.7−3946: IC scattering on the cosmic microwave background by relativistic electrons (leptonic model) and π^0-decay gamma rays resulting mainly from inelastic collisions between relativistic protons and ambient gas nuclei (hadronic model). It is generally accepted that DSA operates at SN shocks producing high-energy protons and electrons. However, injection mechanisms of supra-thermal particles are poorly known so that the current theory cannot tell us about the number of relativistic protons and electrons produced at shocks. This makes it difficult to reliably predict the levels of leptonic and hadronic gamma rays.

The lack of thermal X-ray lines provided a stringent constraint on the gamma-ray production mechanisms. The luminosity of hadronic gamma rays scales as $\bar{n}_H W_p$, where $\bar{n}_H$ denotes the gas density averaged over the emission volume (where accelerated protons are assumed to be uniformly distributed), $W_p = \xi E_{SN}$ is a total energy content of accelerated protons, and $E_{SN} \sim 10^{51}$ erg is the total kinetic energy released by the SN explosion. The lack of thermal X-ray emission in SNR RX J1713.7−3946

(Slane et al. 1999; Tanaka et al. 2008) severely restricts the gas density in the SNR to be small. Ellison et al. (2010) have performed calculations of thermal X-ray emission from shocked plasma with non-equilibrium ionization in the case of uniform ambient density, following a hydrodynamic evolution with which nonlinear DSA theory is coupled; they found that the shocked gas densities required for consistency with the hadronic model are $n_H \lesssim 0.2$ cm^{-3}. It should be noted that, taking $E_{SN} = 2 \times 10^{51}$ erg, one needs $\xi \sim 1$ (i.e., extremely efficient acceleration) for $\bar{n}_H = 0.1$ cm^{-3} and $d = 1$ kpc. The extremely efficient (more efficient than usually assumed) transformation of the SN kinetic energy into accelerated particles may lead to very low shocked gas temperature (Drury et al. 2009), which in turn could change the density requirement.

The measurements of GeV gamma-ray emission obtained with the *Fermi*-LAT presented in this paper provide new, crucial information about the particle population responsible for the gamma-ray emission. We have measured the gamma-ray spectrum of SNR RX J1713.7−3946 in the energy range from 500 MeV to 400 GeV and found that the spectrum can be characterized by a hard power law with photon index $\Gamma = 1.5 \pm 0.1$(stat)± 0.1(sys), smoothly connecting with the steeper TeV gamma-ray spectrum measured with H.E.S.S. Note that the measured gamma-ray spectrum of RX J1713.7−3946 now covers five orders of magnitude in energy, which is unprecedented for SNRs.

The hard power-law shape in the *Fermi*-LAT energy range with photon index of $\Gamma = 1.5 \pm 0.1$ qualitatively agrees with the expected IC spectrum of the leptonic model, as illustrated in both Figures 3 and 4. If the leptonic model explains the gamma-ray spectrum, the *Fermi*-LAT spectrum is emitted by a power-law part of the accelerated electrons, and therefore we can deduce the power-law index of electrons from the measured photon index. Using $\Gamma = 1.5 \pm 0.1$, we obtain $s_e = 2\Gamma - 1 = 2.0 \pm 0.2$. The energy flux ratio of the observed synchrotron X-ray emission and the gamma-ray emission means that the average magnetic field is weak, $B \simeq 10\,\mu G$ (Aharonian et al. 2006; Porter et al. 2006; Ellison et al. 2010). The maximum energy of electrons is then $E_{e,max} \sim 20$–40 TeV as determined from the *Suzaku* X-ray spectrum (Tanaka et al. 2008). The presence of synchrotron X-ray filaments varying on yearly timescales (Uchiyama et al. 2007), if interpreted as being due to fast electron acceleration and synchrotron cooling, requires $B \sim 0.1$–1 mG, which is difficult to reconcile with the weak average field. Alternatively, the X-ray variability may be caused by time-variable turbulent magnetic fields (Bykov et al. 2008) which require a smaller magnetic field strength. The filamentary structures and variability in X-rays should be attributed to locally enhanced magnetic fields in the case of the leptonic model (Pohl et al. 2005).

As shown in Figure 3, several groups have previously presented calculations of IC gamma-ray spectra. Detailed comparisons between the observed total GeV–TeV spectrum and IC models show that none of the previous IC models matches exactly with the data. Some additional complications would need to be introduced to realize a better description of the gamma-ray data. For example, the shape of the total IC spectrum could be modified if we add a second population of electrons (or even multiple populations) which has a different maximum energy (see Tanaka et al. 2008; Yamazaki et al. 2009). Another way of modifying the IC spectral shape is by invoking more intense interstellar radiation fields, though this would require a substantial increase in the photon density (see Tanaka et al. 2008).

Even in the case of the leptonic model, it is important to constrain the level of π^0-decay emission at GeV energies by allowing for a hybrid (leptonic and hadronic) model of the GeV–TeV gamma-ray spectrum. For proton number index $s = 2$ (assumed to be same as the electron number index: see, e.g., Baring et al. 1999 for a discussion of why relativistic electron and ion indices should be very similar in non-linear shocks), the GeV flux upper limit at 1 GeV corresponds to $W_p < 0.3 \times 10^{51}(\bar{n}_{\rm H}/0.1\ {\rm cm}^{-3})^{-1}$ erg for $d = 1$ kpc, where $\bar{n}_{\rm H}$ denotes the hydrogen number density of X-ray-/gamma-ray-emitting gas. Therefore, the leptonic model does not necessarily mean the proton content in this SNR is unexpectedly small.

The GeV measurements with *Fermi*-LAT do not agree with the expected fluxes around 1 GeV in most hadronic models published so far (e.g., Berezhko & Völk 2010). Given the current models of DSA, we can disfavor the hadronic origin of the GeV–TeV gamma-ray emission. The proton number index $s \sim 1.5$ inferred by the LAT spectrum is as small as the asymptotic index of $s = 1.5$ predicted by extremely efficient CR acceleration (Malkov 1999; see also Ellison & Eichler 1984 for early indications of this limiting behavior). Unless this asymptotic index is realized in the shock waves of RX J1713.7−3946, the hard *Fermi*-LAT spectrum cannot be ascribed to the π^0-decay emission. However, such a proton energy distribution is not observed in the current models of efficient DSA (Ellison et al. 2010).

4. SUMMARY

We have measured the GeV gamma-ray emission from RX J1713.7−3946 with the *Fermi*-LAT. The emission is extended and shows a size that matches the TeV-detected gamma-ray emission from this SNR. The gamma-ray spectrum for the SNR has been measured over more than five orders of magnitude combining *Fermi*-LAT and H.E.S.S. observations. The spectral index in the *Fermi*-LAT band is very hard with a photon index of 1.5 ± 0.1 which is well in agreement with emission scenarios in which the dominant source of emission is IC scattering of ambient photon fields of relativistic electrons accelerated in the shock front. The dominance of leptonic processes in explaining the gamma-ray emission does not mean that no protons are accelerated in this SNR, but that the ambient density is too low to produce a significant hadronic gamma-ray signal. RX J1713.7−3946 is the first remnant where the combination with H.E.S.S. data yields spectroscopic measurements over more than five decades in energy that, in contrast to many of the other LAT-detected remnants, suggests a leptonic origin of the gamma-ray emission.

REFERENCES

Abdo, A. A., et al. 2009a, Phys. Rev. D, 80, 122004
Abdo, A. A., et al. 2009b, ApJ, 696, 1084
Abdo, A. A., et al. 2010a, ApJS, 188, 405
Abdo, A. A., et al. 2010b, ApJ, 710, L92
Abdo, A. A., et al. 2010c, Phys. Rev. Lett., 104, 101101
Acero, F., et al. 2009, A&A, 505, 157
Aharonian, F., et al. 2006, A&A, 449, 223
Aharonian, F., et al. 2007, A&A, 464, 235
Albert, J., et al. 2007, A&A, 474, 937
Atwood, W. B., et al. 2009, ApJ, 697, 1071
Baring, M. G., Ellison, D. C., Reynolds, S. P., Grenier, I. A., & Goret, P. 1999, ApJ, 513, 311
Bell, A. R. 1978, MNRAS, 182, 147
Berezhko, E. G., & Völk, H. J. 2006, A&A, 451, 981
Berezhko, E. G., & Völk, H. J. 2010, A&A, 511, A34
Blandford, R. D., & Ostriker, J. P. 1978, ApJ, 221, L29
Bykov, A. M., Uvarov, Y. A., & Ellison, D. C. 2008, ApJ, 689, L133
Cassam-Chenaï, G., et al. 2004, A&A, 427, 199
Castro, D., & Slane, P. 2010, ApJ, 717, 372
Dame, T. M., Hartmann, D., & Thaddeus, P. 2001, ApJ, 547, 792
Drury, L., Aharonian, F. A., Malyshev, D., & Gabici, S. 2009, A&A, 496, 1
Ellison, D. C., & Eichler, D. 1984, ApJ, 286, 691
Ellison, D. C., Patnaude, D. J., Slane, P., & Raymond, J. 2010, ApJ, 712, 287
Ellison, D. C., & Vladimirov, A. 2008, ApJ, 673, L47
Fukui, Y., et al. 2003, PASJ, 55, L61
Gotthelf, E. V., et al. 2001, ApJ, 552, L39
Green, D. A. 2004, Bull. Astron. Soc. India, 32, 335
Hwang, U., et al. 2004, ApJ, 615, L117
Jones, F. C., & Ellison, D. C. 1991, Space Sci. Rev., 58, 259
Katz, B., & Waxman, E. 2008, J. Cosmol. Astropart. Phys., JCAP01(2008)018
Koyama, K., et al. 1997, PASJ, 49, L7
Lazendic, J. S., et al. 2004, ApJ, 602, 271
Malkov, M. A. 1999, ApJ, 511, L53
Malkov, M. A., & Drury, L. 2001, Rep. Prog. Phys., 64, 429
Mattox, J. R., et al. 1996, ApJ, 461, 396
Moriguchi, Y., et al. 2005, ApJ, 631, 947
Morlino, G., Amato, E., & Blasi, P. 2009, MNRAS, 392, 240
Pfeffermann, E., & Aschenbach, B. 1996, in Proc. Roentgenstrahlung from the Universe, ed. H. U. Zimmermann, J. H. Trümper, & H. Yorke, 267
Pohl, M., Yan, H., & Lazarian, A. 2005, ApJ, 626, L101
Porter, T. A., Moskalenko, I. V., & Strong, A. W. 2006, ApJ, 648, L29
Rando, R., et al. (for the Fermi LAT Collaboration). 2010, in Astroparticle, Particle, and Space Physics, Detectors and Medical Physics Applications, ed. C. Leroy et al., 790
Slane, P., et al. 1999, ApJ, 525, 357
Tanaka, T., et al. 2008, ApJ, 685, 988
Uchiyama, Y., Aharonian, F. A., & Takahashi, T. 2003, A&A, 400, 567
Uchiyama, Y., et al. 2007, Nature, 449, 576
Wang, Z. R., Qu, Q.-Y., & Chen, Y. 1997, A&A, 318, L59
Yamazaki, R., Kohri, K., & Katagiri, H. 2009, A&A, 495, 9
Zirakashvili, V. N., & Aharonian, F. A. 2010, ApJ, 708, 965